Int. J. Sci. R. Tech., 2026 3(5)
A Multidisciplinary peer-reviewed Journal
www.ijsrtjournal.com [ISSN: 2394-7063]

Original Article

EEG-Based Automated Diagnosis Of Autism Spectrum Disorder Using Discrete Wavelet Transform, Entropy Features And Multilayer Perceptron Neural Network

Romain Atangana[1, 2, 3], Amstrong Emini Me Zenanga[3], Aurelle Tchagna Kouanou[5], Vivien Loick Beyala Kamgang[3,6], Daniel Tchiotsop[1], Daniel Gams Massi[4], Godpromesse Kenne[1]

[1]Unité de Recherche d'Automatique et d'Informatique Appliquée (UR-AIA), IUT of Bandjoun, University of Dschang –Cameroun P. O Box 134 Bandjoun
[2]Unité de Recherche de Matière Condensée d'Electronique et de Traitement du Signal (UR-MACETS), Faculty of Science, University of Dschang-Cameroun, PO Box 67 Dschang
[3]Department of Computer Science, Higher Teacher Training College, University of Bertoua-Cameroun P.O Box 652 Bertoua
[4]Department of Neurology, Faculty of Health Science, University of Buea, B.O Box Buea
[5]Department of Computer Engineering and Telecommunications (at National advanced school of Posts, Telecommunications and ICTs
[6]Department of Mathematics, statistic and computer sciences, the University of Bertoua –Cameroon P.O Box 416 Bertoua

ABSTRACT

Autism Spectrum Disorder (ASD) is a complex neurodevelopmental condition characterized by persistent deficits in social communication and interaction, alongside restricted and repetitive patterns of behavior. Despite its increasing global prevalence, the clinical diagnosis of ASD remains a challenging and time-consuming process, heavily reliant on subjective behavioral assessments conducted by specialized clinicians. This limitation underscores the urgent need for objective, reliable, and automated diagnostic tools. In this study, we propose a computer-aided diagnosis (CAD) system for ASD detection based on the analysis of Electroencephalogram (EEG) signals. The proposed pipeline encompasses EEG signal preprocessing, decomposition into frequency sub-bands using the Discrete Wavelet Transform (DWT), and extraction of discriminative features through four entropy-based measures, namely Logarithmic Energy Entropy, Tsallis Entropy, Rényi Entropy, and Shannon Entropy. The extracted feature vectors are subsequently fed into a Multilayer Perceptron (MLP) neural network trained via the backpropagation algorithm to classify subjects into two categories: ASD patients and neurotypical controls. Experimental evaluations conducted on a dataset of 56 subjects (28 ASD, 28 neurotypical) demonstrate that Shannon Entropy yields the highest classification performance, achieving an accuracy of 98.84%, a sensitivity of 100%, and a specificity of 96%. These results highlight the effectiveness of entropy-based feature extraction combined with MLP classification for the automated diagnosis of ASD from EEG signals, and suggest the potential of the proposed approach as a valuable decision-support tool in clinical neuroscience.

Keywords: Autism Spectrum Disorder (ASD); Electroencephalography (EEG); Discrete Wavelet Transform (DWT); Entropy; Artificial Neural Network (ANN); Multilayer Perceptron (MLP); Backpropagation Algorithm; Computer-Aided Diagnosis.

INTRODUCTION

Autism Spectrum Disorder (ASD) is a lifelong neurodevelopmental condition characterized by persistent impairments in social communication and interaction, restricted and repetitive behavioral patterns, and atypical sensory processing [1]. Clinical manifestations typically emerge during the first years of life, with early signs including delayed language

Relevant conflicts of interest/financial disclosures: The authors declare that the research was conducted in the absence of any commercial or financial relationships that could be construed as a potential conflict of interest.

acquisition, limited social reciprocity, and stereotyped behaviors [2]], [3]. According to the World Health Organization (WHO), ASD affects approximately 1 in 100 children worldwide, making it one of the most prevalent neurodevelopmental disorders of our time, with significant implications for affected individuals, families, and healthcare systems.

Despite its widespread prevalence, the diagnosis of ASD remains a complex and inherently subjective process. Current diagnostic protocols, such as the Autism Diagnostic Observation Schedule (ADOS) and the Autism Diagnostic Interview-Revised (ADI-R), rely exclusively on behavioral observation and cognitive assessment conducted by experienced clinicians [3]. A well-documented clinical observation indicates that autistic children at approximately 24 months of age are typically unable to produce two meaningful words spontaneously, without imitation or echolalia. However, the subtlety of early neurological impairments makes timely and accurate detection particularly challenging, and the precise etiological factors underlying ASD remain incompletely understood.

In this context, neurophysiological biomarkers have attracted growing research interest as objective complements to behavioral diagnosis. The Electroencephalogram (EEG) has emerged as one of the most promising modalities for ASD characterization, owing to its high temporal resolution — on the order of milliseconds — non-invasiveness, and ability to capture real-time cortical dynamics in both resting and task-related states [4], [5]. EEG signals encode neural activity across five canonical frequency bands: delta (0–4 Hz), theta (4–8 Hz), alpha (8–16 Hz), beta (16–32 Hz), and gamma (32–64 Hz), each associated with distinct cognitive and physiological functions. The delta band is predominantly active during deep sleep and attentional processes; theta is linked to memory encoding and drowsiness; alpha reflects relaxed wakefulness and cognitive inhibition; beta is associated with active thinking, alertness, and motor control; and gamma underlies early sensory processing and feature binding [5].

Converging evidence from multiple studies indicates that ASD is associated with measurable alterations in EEG spectral profiles and connectivity patterns. Children with ASD consistently exhibit atypical neural activity across frequency bands during sensory stimulation paradigms, along with reduced short-range connectivity in the left hemisphere — a region critically involved in language processing — and paradoxically increased long-range connectivity between distant cortical regions [6]. Furthermore, a significant proportion of individuals with ASD present with epileptiform EEG abnormalities, suggesting underlying neurological disruptions that extend beyond behavioral manifestations [6]. Molholm and colleagues further emphasized that EEG-derived biomarkers could not only quantify the severity of autistic symptoms but also contribute to earlier and more objective diagnosis, with early intervention being strongly associated with improved long-term outcomes [6].

These observations have motivated a growing body of research into machine learning-based, computer-aided diagnosis (CAD) systems for ASD, leveraging EEG signal processing as a non-invasive, cost-effective, and objective diagnostic pathway [7]. In this study, we propose a CAD framework combining Discrete Wavelet Transform (DWT)-based frequency decomposition, entropy feature extraction, and Multilayer Perceptron (MLP) neural network classification to discriminate ASD patients from neurotypical controls. The remainder of this paper is organized as follows: Section II reviews related works; Section III describes the materials and methodology; Section IV presents the experimental results; Section V discusses the findings; and Section VI concludes the paper.

II RELATED WORKS

Jeyabose and colleagues presented a robust and interpretable convolutional deep learning framework for early ASD detection from resting-state EEG signals, with a particular emphasis on explainability — an increasingly critical requirement for clinical deployment of AI-based diagnostic tools. The proposed system converts resting-state EEG recordings into time-frequency spectrogram images, which are subsequently processed by a deep convolutional architecture trained to discriminate ASD from neurotypical patterns. The framework was validated across two independent cohorts: the KAU dataset from King Abdulaziz University and the ACE

dataset available through the NIH National Database for Autism Research (NDA). Beyond achieving high diagnostic performance, the system incorporates Explainable AI (XAI) visualization techniques that provide actionable insights into the neural substrates underlying ASD, enhancing both the transparency and the clinical interpretability of the model's decisions, thereby facilitating its integration into real-world diagnostic workflows.

Shi and colleagues introduced TFSNet, a time-frequency synergy network designed to address the limitations of existing methods in capturing time-varying dynamics and joint time-frequency representations from EEG signals for ASD classification. The proposed architecture incorporates three key components: a Temporal Dynamic Residual Block (TDRB) for enhanced time-domain feature extraction; a Short-Time Fourier Transform (STFT) module combined with a convolutional attention mechanism for frequency-domain feature capture; and an Adaptive Cross-Domain Attention (ACDA) mechanism for efficient fusion of time-frequency representations. The framework was evaluated on two independent benchmark datasets — the University of Sheffield dataset (28 ASD, 28 neurotypical controls) and the King Abdulaziz University (KAU) dataset (12 ASD, 5 controls) — achieving average classification accuracies of 98.68% and 97.14%, respectively, significantly outperforming existing machine learning and deep learning approaches on both benchmarks.

Tang and colleagues proposed a resting-state EEG-based hybrid graph convolutional network framework, referred to as Rest-HGCN, for automated ASD diagnosis. The model integrates brain network analysis techniques with data-driven learning strategies to extract discriminative graph features from resting-state EEG signals. By jointly leveraging cognitive prior knowledge-based graph components and adaptively learned data-driven components, Rest-HGCN effectively captures differential brain connectivity patterns between neurotypical children and ASD patients. An attention mechanism was further incorporated to enable efficient integration of these complementary feature streams. The model was evaluated through k-fold cross-validation on the publicly available ABC-CT resting-state EEG dataset, comprising 399 participants (280 ASD and 119 neurotypical controls), achieving classification accuracies of 87.12% in single-subject experiments and 85.32% in cross-experiment validation, demonstrating robust generalizability across subjects.

Louise Bogéa Ribeiro et al (2023) This study aimed to evaluate functional connectivity and spectral power using EEG signals. EEG records the brain activity of an individual by displaying wavy lines that depict brain cells communication through electrical impulses. The study suggests that EEG is useful in diagnosing ASD by evaluation entropy in the brain and that researchers may be able to develp new diagnostic methos for ASD which focuses on particular stimuli and brainwaves if they conduct more extensive studies withj higher numbers and more rigorous study designs.

Véronique D. Thérien et al (2023) Authors investigated the brain correlaties underlying visual segmentation associated with the well-established autistic- superior visuospatial abilities in distinct sub groups using functional magnetic resonance imaging. Participants completed a computerized adapted BD task with …..

Pilar Garcés et al (2022) The authors quantified resting state EEG alpha peak metrics, power spectrum (PS , 2-32 Hz, and functional connectivity (FC) in 411 children, adolescents and adults (n=212 ASD, n=199 neurotypicals (NT) all with IQ > 75. They performed analyses in source-space using individual head models derived from the participants MRIs. They tested for differences in mean and variance between the ASD and NT groups for both PS and FC using linear mixed effects models accounting for age, sex, IQ and site effects. In the training dataset they found an interaction between age and group for the reactivity to eye opening and a significant but weak multivariate ASD vs NT classification performance for PS and FC, sensitivity 52%- 62%, specificity 59% - 73%.

Katia Ggnon, Christianne Bolduc et al (2021) Authors tested the hypothesis of an atypical scalp distribution of electroencephalography (EEG) activity during Rapid Eye Movement (REM) sleep in young autistic adults. EEG spectral activity and ratio along the anteroposterior axis and across hemispherres were compared in 16 neutypical (NT) young adults 17 individuals with autism spectrum disorder (ASD). EEG spectral power was lower in the ASD group over the bilateral, central and right parietal (beta activity as

well as bilateral occipital (beta, theta) and total activity recording sites. EEG activity thus appears to be atypical distributed over the scalp surface in young with autism during REM sleep within cerebral hemispheres, and this correlates with some ASD symptoms.

Nur Alisa Ali et al (2020) this work aimed to reveal the different pattern between autistic and normal children via electroencephalogram EEG signal by using the deep learning algorithm. The brain signal database used pattern recognition algoritm where the extracted features will undergo the multilayer perceptron neural network for classification process. The promising methode to perform the classification is through a deep learning algorithm which is currently a well-known and superior method in the pattern recognition field. The higher percentage means the more effectiveness for the ASD diagnosis.

Heather L. Green et al (2020) The mismatch negativity (MMN), a passive auditory evoked potential, offers insight into the brain's ability to direct attention to novel sounds. Since exposure to speech is necessary for learning to map meaning onto phenomenes, the author predicted slower MMN responses to speech sounds would indicate presence of language impairment in ASD. Authors explored the relationship between MMN latency in children ages 5 -10 with ASD plus language impairment (ASD +LI), ASD minus language impairment (ASD-LI), typically developping children (TD) during an auditory oddball experiment presenting speech and pure tone sounds. Contrary to their prdiction, children with ASD+LI demonstrated decreased MMN latency in the left hemisphere in response to novel vowel sounds compared to children with ASD-LI and TD controls.

Jia Wang et al (2020) Here, EEG coherence analysis was used in a cohort of childern with ASD (n=13) and matched typically developing controls TD (n=15) to examine the functional connectivity characteristics in long-distance and short – distance electrode pairs. Subsequently, they explore the association between the connectivity strength of coherence and system severity in cildren with ASD. Compared with TD group, individuals with ASD showed increased coherence in short-distance electrode pairs in the right temporal-parietal region (delta, alpha, beta bands) right central parietal region (theta, alpha, beta bands), occipital region (theta, alpha, beta bands), right central-parietal region (delta, alpha, betabands), and the prefrontal region (only beta band). In long distance coherence analysis, ASD group showed increased coherence in bilateral frontal region, temporal region, parietal regions, and frontal-occipatal region in alpha and beta bands; the strength of such, connections was associated with symptoms severity.

Stromo Ibrahim et al (2018) in this work authors investigate different electroencephalography (EEG) feature extraction and classification techniques to assist in the diagnosis on both epilepsy and autism spectrum disorder (ASD). First, the EEG signal is preprocessed to remove major artifacts before being decomposed into several EEG- sub bands using a discrete-wavelet transform (DWT). Two non-linear methods were studied: Shannon entropy and Largest Lyapunov exponent, which mesure complexity and chaoticity in EEG recording in addition to the two conventional methods (namely, Standard deviation, and band power). The combination of DWT, Shannon entropy, K-nearest neighbor (KNN) technique produces the most promising classification result, with an overall accuracy of up to 94,6 % for the three class classification problems.

Ridha Djemal et al (2017), In this work, a new computer aided diagnosis of autism based on electroencephalography (EEG) signal analysis is investigated. The method is based on discrete wavelet transform (DWT), entropy (En) and artificiel neural networok (ANN). DWT is used to decompose EEG signal into approximation and details coefficients to obtain EEG subbands. The feature vector is constructed by computing Shannon entropy values from each EEG sub band. ANN classifies the corresponding EEG signal into normal or autistic based on the extracted features. The experimental results show the effectiveness of the proposed method for assisting autism diagnosis.

Marjolaine chicoine et al (2013) The sleep of 34 adults (16 autistics) and 26 children (13 autistics) was recorded. Sleep spindles were counted and compared between groups at prefrontal (Fp1, Fp2) and central (C3, C4) electrodes. Both diagnostic groups showed a similar decrease in sleep spindle with age. Autistic children had significantly less spindles than controls

at Fp2 and C4, adults with autism had significantly less spindles than controls at the two central electrodes.

III MATERIALS AND METHOD

3.1 Materials

This section describes the hardware and software resources employed throughout the development and implementation of the proposed ASD diagnostic system.

3.1.1 Hardware Configuration

All experiments and signal processing computations were carried out on a personal computer equipped with an Intel Core i5-7200U dual-core processor clocked at 2.70 GHz, 8 GB of DDR4 RAM, and 1 GB of dedicated graphics memory. While modest by modern high-performance computing standards, this configuration was deliberately chosen to reflect a realistic and accessible hardware environment, thereby demonstrating the practical deployability of the proposed approach in resource-constrained clinical settings such as those commonly found in sub-Saharan African healthcare facilities.

3.1.2 Software Environment: MATLAB

All signal processing, feature extraction, classification, and performance evaluation procedures were implemented using MATLAB R2021a (MATrix LABoratory), developed by MathWorks Inc. MATLAB is a high-level, matrix-oriented scientific computing environment specifically designed to streamline numerical computation, algorithm development, and data visualization. Its unified workspace integrates a code editor, an interactive command console, and a step-by-step debugging tool, enabling efficient iterative development and rapid prototyping of signal processing pipelines.

A key advantage of MATLAB for biomedical signal processing lies in its extensive ecosystem of domain-specific toolboxes. In this work, the Signal Processing Toolbox was leveraged for EEG filtering and spectral analysis, while the Deep Learning Toolbox provided the infrastructure for designing, training, and evaluating the Multilayer Perceptron (MLP) neural network classifier. The Wavelet Toolbox was additionally used to implement the four-level Discrete Wavelet Transform (DWT) decomposition central to the feature extraction stage. The EEGLAB plug-in, an open-source MATLAB toolbox widely adopted in the neuroscience community, was further employed for EEG data import, preprocessing, artifact rejection via Independent Component Analysis (ICA), and signal segmentation. Together, these tools provided a coherent, reproducible, and well-validated computational framework for the end-to-end implementation of the proposed diagnostic pipeline.

3.2 Methodology

This part presents the steps that were followed to achieve the creation of the model allowing automatic daignosis.

3.2.1 Flowchart of the work

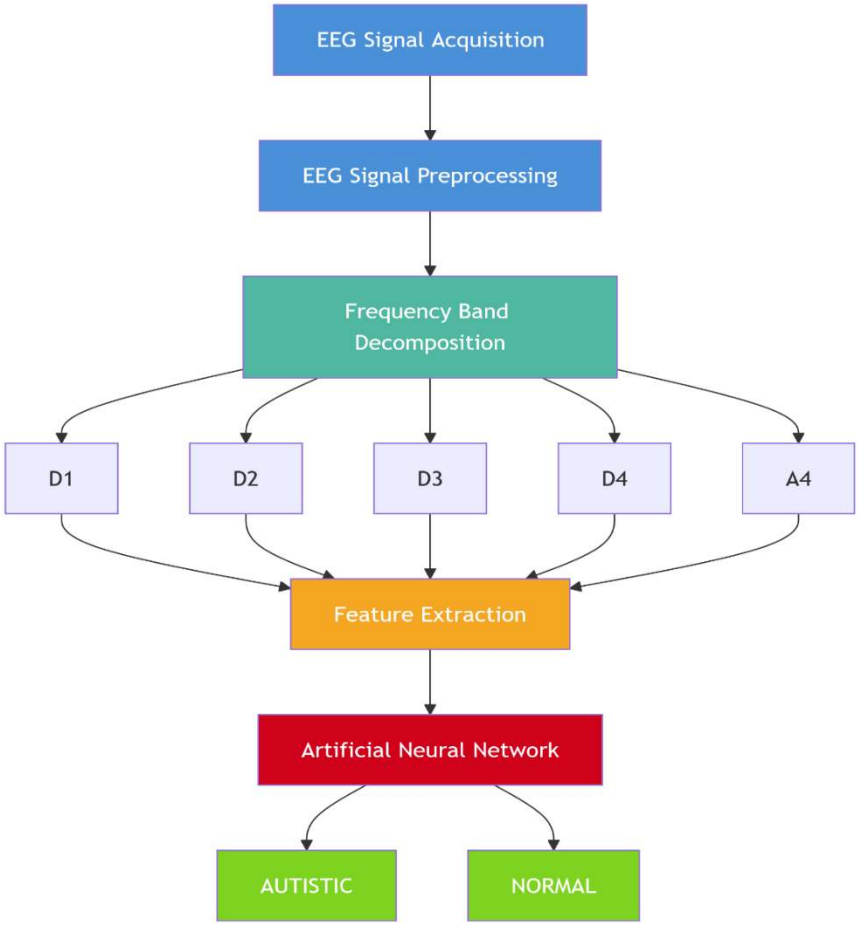

Figure 1 : flow chart of the work

Figure 1 provides a comprehensive overview of the proposed methodology. The pipeline begins with a preprocessing stage applied to the raw EEG signals, which encompasses bandpass filtering and signal segmentation. This step is primarily dedicated to the removal of physiological artifacts—including electrocardiographic (ECG), electrooculographic (EOG), and electromyographic (EMG) signals—as well as the suppression of electrode contact noise and other environmental interferences.

Following preprocessing, the segmented EEG epochs are subjected to a discrete wavelet transform (DWT)-based decomposition. This process yields both detail coefficients (D1–D4) and approximation coefficients (A4), corresponding to the five canonical EEG frequency sub-bands: delta, theta, alpha, beta, and gamma.

In the feature extraction phase, a set of entropy-based measures is computed directly from the original EEG segments as well as from the resulting wavelet coefficients. These entropy features are employed to characterize the temporal distribution of the signals and to reduce the dimensionality of the feature space. Additionally, conventional statistical attributes—such as the mean and standard deviation—are extracted to complement the entropy-based descriptors.

Finally, the resulting feature vectors are fed into an artificial neural network (ANN), which serves as the classification engine to distinguish between autistic and neurotypical subjects.

3.2.2 Dataset acquisition

The EEG dataset was acquired via the Biosemi Activetwo EEG system. The originals recordings were converted into. set and .fdt files via EEGLAB. There is a .fdt file and a .set file for each recording. The .fdt file contains the data, the .set file contains information about about the recording settings. The files can be opened in the EEGLAB Software. Data was acquired from 28 people with a diagnosis of autism spectrum disorder and 28 neurotypical controls aged from 18 to 68. The paradigme that

generated data used a period of 2,5 minute (150 second) at rest with eyes closed.

3.2.3 Preprocessing of EEG signals.

EEG signals are usually cluttered with noises derived from many factors such as poor electrode placement, dirty scalp, magnetic field of the device, blood pressure, respiration, heart and muscle activities [6] Preprocessing therefore aims to remove these artifacts to be able to carry out a good analysis. For this, i twill be necessary to filter the EEG data which will improve the stability and increase the precision, the nit will be necessary to normalize the signals and finally to remove these artifacts.

3.2.3.1 Filtering

Before the operation of filtering, we reduced the samplingrate from 212 Hz to 256 Hz, this is to reduce space and calculation time. The impulse response filter was applied; this helps to eliminate high frequencies. The highest frequency was set at 64 Hz

3.2.3.2 Normalization

During EEG data collection, the resistance of each electrode changes over time, time which causes changes in voltage readings. As a result, the variances of some channels may be significantly different from those of others. The normalization process not only improves the classification performances, but also solves the non-stability problem. In the EEGLAB toolbox, we used the normalization function.

3.2.3.3 Artifacts removal

It is mandatory to remove all artifacts and improve the signal-to-nois ratio by filtering the acquired data. We used independent component analysis (ICA) for the removal of ocular artifacts. Electrodes FP1, FP2, F7 and F8 are used as reference signals for ocular artifact suppression. After these steps, all EEG signals were segmented into 20 seconds. The work was carried out using MATLAB EEGLAB Toolbox. The FPz electrode is used as a reference electrode for the diagnosis of autism.

3.2.4 Mathematical principles

3.2.4.1 EEG signals decomposition into frequency bands

The discrete wavelet transforms analysis of the EEG signals carry out intended to decompose these EEG signals into frequency bands (δ, α, β, θ et γ). Wavelet transform (WT) techniques are widely used in EEG signals processing for time-frequency decomposition. There are two types of wavelets transform continuous wavelet transform (CWT) and discrete wavelet transform (DWT) [2].

The continuous wavelet transform (CWT) of the signal x(t) is defined as follows

$$TOC_{a,b}(x) = \frac{1}{\sqrt{|x|}} \int x(t)\, \Psi^{*}\left(\frac{t-b}{a}\right) dt \qquad (1)$$

In this expression $\Psi^{*}(t)$ is called mother wavelet function while a and b dilatation (scale) and translation parameters respectively are real numbers. However, an obvious disadvantage of the CWT technique is that it requires excessive calculations. Therefore, we used but (DWT) in the proposed work to decompose a given signal into approximation and detail coefficients.

The discrete wavelet transform (DWT) is defined using the discrete value of parameters a and b as follows

$$TOD_{m,n}(x) = a_0^{\frac{-m}{2}} \int x(t)\, \Psi\left(a_0^{\frac{-m}{2}} t - nb_0\right) dt \qquad (2)$$

Where m and n (m, n∈Z) indicate the frequency and time location respectively. The approximation coefficients at each level are further decomposed into levels following approximation and detail coefficients as shown in figure 2.

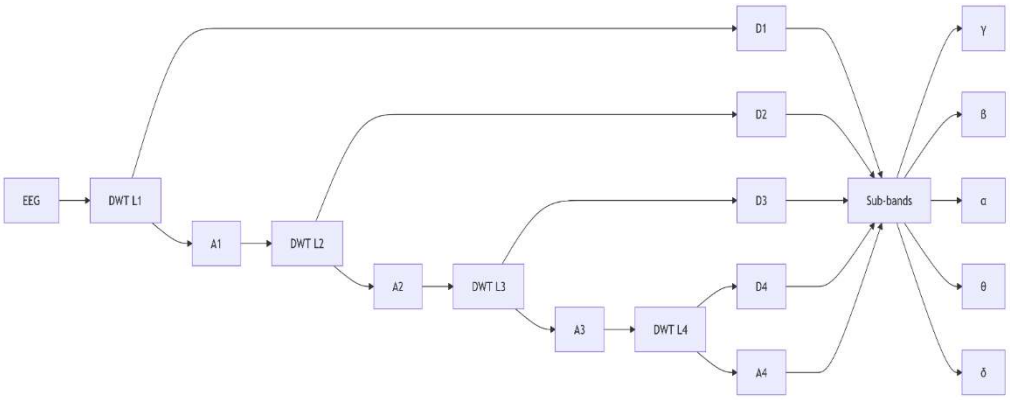

Figure 2 : four- levels (DWT) decomposition into detail and approximation coefficients

Wavelet coefficients	EEG Sub-bands	Frequency (Hz)
D1	Gamma	32-64
D2	Beta	16-32
D3	Alpha	8-16
D4	Theta	4-8
A4	Delta	0-4

Tableau 1: Frequency bands partition

In this work we used the DWT decomposition at 4 levels with Daubechies-four (db4) mother wavelet in order to extract five EEG sub-bands and to achieve better in the feature extrction stage. The characteristics are extracted from the detail coefficients at various levels (D1 … D4) and from approximation coefficient at the last level (A4). The frequency bands of the EEG signals corresponding to the 4-level DWT decomposition with a sampling frequency of 256 Hz on EEG signals are shown in table 1.

As shown in this table, wavelet coefficients correspond to several EEG subbands namely., delta (0-4 Hz), theta (4–8 Hz), alpha (8–16 Hz), beta (16–32 Hz) et gamma (32–64 Hz). Different frequency sub bands can reveal time series characteristics of the EEG signal.

3.2.4.2 Extraction of features

Many features can be extracted from the time series of EEG signals, such as the use of statistical characteristics or non-linear characteristics (entropy). Several previous studies show the effectiveness of using entropy to analyze EEG signal such as Epilepsy diagnosis and autism diagnosis in occurrence. Entropy can be used to measure complexity, regularity and statistical quantification of time series data such as EEG.

Bosi et al. [7] investigated the possibility of using EEG complexity as a biomarker of ASD risk. Nonlinearity and abnormal complexity of brain signal may reveal disorders brain or cognitive disorders. So, we will also use some entropy functions to extract features.

i. Logarithmic energy entropy

This entropy is a type of wavelet entropy. Assume a signal $x = [x_1 x_2 x_3 x_5 \dots x_n]$, a probability distribution function denoted $p(x_i)$ where i is the index of the signal elements. Logarithmic energy is defined as follows

$$H = \sum_{i=1}^{n} log\ (p_i^2) \qquad (3)$$

ii. Tsallis's Entropy

In physics, the Tsallis entropy is a generalization of the standand entropy of Boltzmann-Gibbs. Given a probability $\{p_i\}$, with the condition $\sum p_i = 1$ and for all real number q , the Tsallis entropy is defined as

$$H = \frac{k}{q-1}\left(1 - \sum_i p_i^{\alpha}\right) \quad (4)$$

Where q is the entropy index parameter and k a positive constant.

iii. Renyi's Entropy

Renyi's entropy is a statistical function used to measure diversity and randomness of the distribution of the discrete signal and to estimate the uncertainty of the discrete signal. It can be calculated by the following formula

$$H = \frac{1}{1-\alpha} log\left(1 - \sum_{i=1}^{n} p_i^{\alpha}\right) \quad (5)$$

where α is the order of the Renyi function, α>0, α#0, et p the probability of the discrete variables from the signal.

iv. Shannon Entropy

this entropy is the technique used to expect the average value of the information containing in the signal and to measure the average uncertainty of the discrete signal. We used the basic shannon entropy developed by Shannon [8]. for a given time, series data $X = [x_1 x_2 x_3 x_5 \dots x_n$ the entropy value can be calculated by the following formula

$$H = -\sum_{i=1}^{k} p_i * log_2(p_i) \quad (6)$$

Where k is the number of unique values in the data X and p_i is the probability for these unique values.

3.2.4.3 Artificial Neural Network (ANN)

a. Architecture of the Network

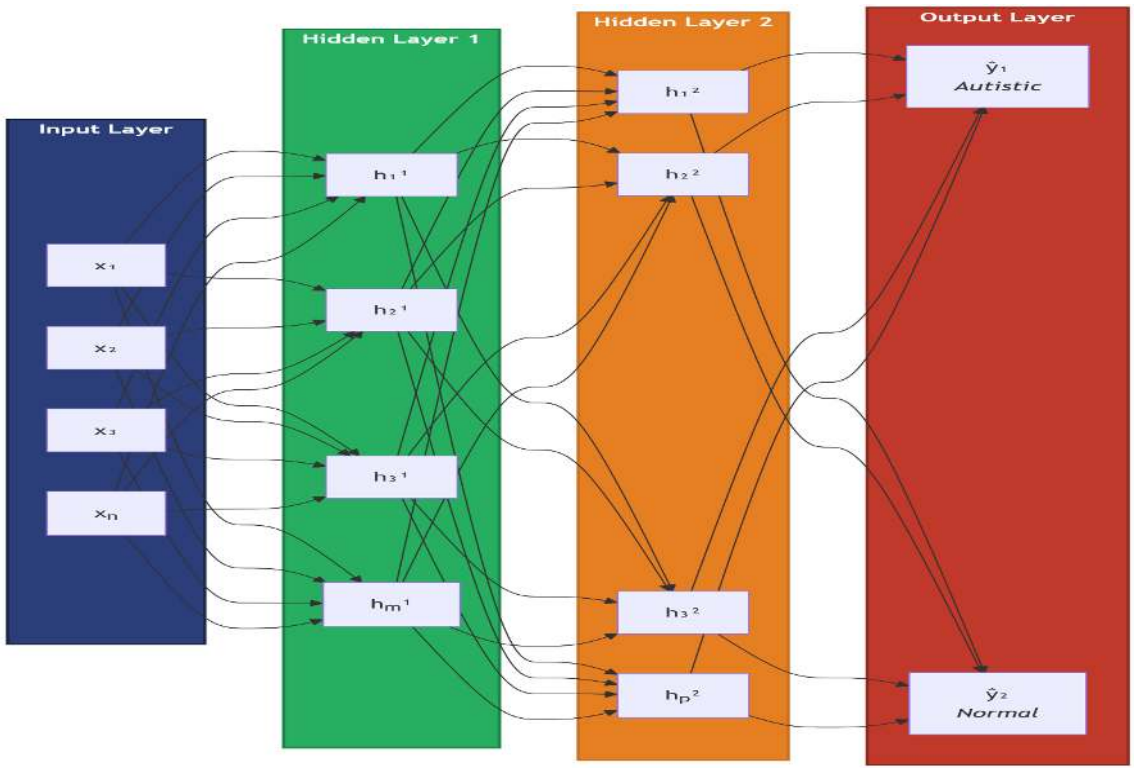

Figure 3 Architecture of the MLP

In the context of biomedical signal processing, particularly with application to EEG signals, classification of data into feature space is often required. The objective of classification is to draw a boundary between two or more classes and labelling them based on their feature. The task being to assign an input pattern represented by a feature vector to one or more pre-defined classes.

Here the MLP classifier consists of an input layer made of 4 neurons, a hidden layer made of 4 neurons and an output layer of 2 neurons.

b. Learning process

We will focus on supervised learning in which the backpropagation algorithm is implemented to update weights by backwarding output error to allow the network to provide answers as close as possible to the known correct answers

c. Activation function

In this work we use the sigmoid function which is defined as follows

$$\varphi(x) = \frac{1}{1+e^{-x}} \qquad (7)$$

Backpropagation algorithm

Learning through gradient descent :

Output layer: Correction is guided by the error between the actual output and the real output.

Hidden layers: Updating weights according to the influence of the error of each output neurone to each hidden neurone

Output values of output neurones :

y_j^t is the value of the j[th] neurone tto the input data X^t :

$$y_j^t = f(a_t^j) = f\left(\sum_{i=1}^{R} \omega_{i,j} * y_i^t + \omega_{j,0}\right) \qquad (8)$$

f is the neurone activation function,

$a_t^j = \sum_{i=1}^{R} \omega_{i,j} * y_i^t + \omega_{j,0}$: is the weighted som of the input neurones plus biais.

$\omega_{i,j}$: weight between the j [th] neurone and the i[th] neurone of the previous layer.

$\omega_{j,0}$: biais of the j[th] neurone;

y_i^t : Output of the i[th] neurone of the previous layer for the input data X ;

R : number of neurones on the previous layer ;

- Output error toward the output layer:

Input Data $\aleph = \{x^t, r^t\}_{t=1}^{N}$, with $r^t = [r_1^t, r_2^t, r_3^t, \dots r_k^t]^T = \begin{bmatrix} r_1^t \\ [\dots] \\ r_n^t \end{bmatrix}$, where $r_j^t = 1 \; si \; x_t \in C_j$ et

$r_j^t = 0$ otherwise.

Error observed for data x^t on the jth neurone to the output layer:

$$e_j^t = r_j^t - y_j^t$$

quadratic error observed for the data x^t on all the K neurones of the output layer (one neurone per class) :

$$E^t = \frac{1}{2}\sum_{j=1}^{k} (e_j^t)^2 \qquad (9)$$

Mean error observed for the dataset $\aleph$:

$$E = \frac{1}{N}\sum_{t=1}^{N} E^t \qquad (10)$$

- Correction of the error for the output layer:

Correction of weights through gradient descent of the mean quadratic error.

$$\Delta\omega_{j,i} = -\eta \frac{\partial E}{\partial \omega_{j,i}} = \frac{\partial\left(\frac{1}{N}\sum_{t=1}^{N} E^t\right)}{\partial \omega_{j,i}} \qquad (11)$$

$$\Delta\omega_{j,i} = -\frac{\eta}{N}\sum_{t=1}^{N} \frac{\partial E^t}{\partial \omega_{j,i}} \qquad (12)$$

The error to the jth neurone depend to the neurones of the previous layer .

Learning for the output layer :

Updating of the weights of the output layer

$$\Delta\omega_{j,i} = -\frac{\eta}{N}\sum_{t=1}^{N} \frac{\partial E^t}{\partial \omega_{j,i}} = -\frac{\eta}{N}\sum_{t=1}^{N} \frac{\partial E^t}{\partial e^t} * \frac{\partial e^t}{\partial y_j^t} * \frac{\partial y_j^t}{\partial a_j^t} * \frac{\partial a_j^t}{\partial \omega_{j,i}} \qquad (13)$$

$$\Delta\omega_{j,i} = \frac{\eta}{N}\sum_{t=1}^{N} e_j^t\, y_j^t(1-y_j^t)y_i^t \qquad (14)$$

$$\Delta\omega_{j,0} = \frac{\eta}{N}\sum_{t=1}^{N}\frac{\partial E^t}{\partial\omega_{j,0}} = \frac{\eta}{N}\sum_{t=1}^{N}\frac{\partial E^t}{\partial e_j^t} * \frac{\partial e^t}{\partial y_j^t} * \frac{\partial y_j^t}{\partial a_j^t} * \frac{\partial a_j^t}{\partial\omega_{j,0}} = \frac{\eta}{N}\sum_{t=1}^{N} e_j^t\, y_j^t(1-y_j^t)y_j^t \qquad (15)$$

- Delta rule:

Let δ_j^t, which corresponds to the local gradient of the neurone j for the input data X^t.

$$\delta_j^t = e_j^t y_j^t(1-y_j^t)y_i^t \qquad (16)$$

Then,

$$\Delta\omega_{j,i} = \frac{\eta}{N}\sum_{t=1}^{N}\delta_j^t y_i^t \qquad (17)$$

and,

$$\Delta\omega_{j,0} = \frac{\eta}{N}\sum_{t=1}^{N}\delta_j^t E^t = \frac{1}{2}\sum_{j=1}^{k}(e_j^t)^2 \qquad (18)$$

- Correction of the corresponding error layer:

The gradient of the error of the hidden layer is:

$$\frac{\partial E^t}{\partial\omega_{j,i}} = \frac{\partial E^t}{\partial y_j^t} * \frac{\partial y_j^t}{\partial a_j^t} * \frac{\partial a_j^t}{\partial\omega_{j,i}} \qquad (19)$$

Only, $\frac{\partial E^t}{\partial\omega_{j,i}}$ changes while $\frac{\partial a_j^t}{\partial\omega_{j,i}}$ and $\frac{\partial y_j^t}{\partial a_j^t}$ are the same as on the output layers. The error to one neurone of the hidden layer depends of the error of the K neurones of the following layer (backpropagation of error).

$$E^t = \frac{1}{2}\sum_{j=1}^{k}(e_j^t)^2 \qquad (20)$$

$$\frac{\partial E^t}{\partial y_j^t} = \frac{\partial}{\partial y_j^t}\left[\frac{1}{2}\sum_{j=1}^{k}\left(e_j^t\right)^2\right] = \sum_k e_k^t * \frac{\partial e_k^t}{\partial y_j^t} \qquad (21)$$

$$\frac{\partial E^t}{\partial y_j^t} = \sum_k e_k^t * \frac{\partial e_j^t}{\partial a_j^t} * \frac{\partial a_j^t}{\partial y_j^t} = \sum_k e_k^t * \frac{\partial[r_k^t - y_k^t]}{\partial a_j^t} * \frac{\partial\left[\sum_k \omega_{k,j} * y_k^t + \omega_{k,0}\right]}{\partial y_j^t} \qquad (22)$$

$$\frac{\partial E^t}{\partial y_j^t} = \sum_k e_k^t[-y_t^k(1-y_t^k)] * \omega_{k,j} \qquad (23)$$

$$\delta_k^t = e_k^t\left[-y_t^k\left(1-y_t^k\right)\right] \qquad (24)$$

$$\frac{\partial E^t}{\partial y_j^t} = -\sum_k \delta_k^t\,\omega_{k,j} \qquad (25)$$

➢ Correction of the corresponding error:

$$\frac{\partial E^t}{\partial \omega_{j,i}} = \frac{\partial E^t}{\partial y_j^t} * \frac{\partial y_j^t}{\partial a_j^t} * \frac{\partial a_j^t}{\partial \omega_{j,i}} = -\left[\sum_k \delta_k^t \, \omega_{k,j}\right] * y_j^t(1 - y_j^t) y_j^t \qquad (26)$$

$$\delta_j^t = e_j^t(1 - y_j^t) \sum_k \delta_k^t \, \omega_{k,j} \qquad (27)$$

$$\Delta\omega_{j,i} = -\eta * \frac{\partial E^t}{\partial \omega_{j,i}} = -\frac{\eta}{N} \sum_{t=1}^{N} \frac{\partial E^t}{\partial \omega_{j,i}} = \frac{\eta}{N} \sum_{t=1}^{N} \delta_j^t y_i^t \qquad (28)$$

$$\Delta\omega_{j,0} = -\eta * \frac{\partial E^t}{\partial \omega_{j,0}} = -\frac{\eta}{N} \sum_{t=1}^{N} \frac{\partial E^t}{\partial \omega_{j,0}} = \frac{\eta}{N} \sum_{t=1}^{N} \delta_j^t \qquad (29)$$

The backpropagation algorithm can be summarized through the following steps:

Step 1: Normalize the training data $X_i^t \in [-1, 1]$ and the real outputs

$r_i^t \in \{0.05; 0.95\}$.

- Step 2: Initialize the weights and the biais to the small random values, $\omega_{j,i} \in U(-0.5,\ 0.5)$;
- Step 3: Select the architecture of the network (the number of hidden layer and the number of neurones per layer);
- Step 4: Choose the neurone activation functions, which can be uniformed or different from one layer to another;
- Step 5 : Select the pair training data real outputs and apply the input vector to the network then let propagate the signal foward through the network.
- Step 6 : Calculate the output of the network in term of the initial weights and the training data set;
- Step 7 : calculate the error between the actual outputs and the real;

$e_j^t = r_j^t - y_j^t$, avec j=1, 2,….,K; t=1,2,…..,N

- Step 8 : Propagate the error backward and update the weights to minimaze the error. Do this for all dataset by starting to the output layer and come gradually to the input layer.;

$$\omega_{j,i} = \omega_{j,i} + \Delta\omega_{j,i} = \omega_{j,i} + \frac{\eta}{N} \sum_{t=1}^{N} \delta_j^t y_i^t \qquad (30)$$

Where the local gradient or Delta is defined as:

$$\delta_j^t = \begin{cases} e_j^t y_j^t(1 - y_j^t), & if\ \ j\ belong\ to\ the\ \ output\ layer \\ y_j^t(1 - y_j^t) \sum_k \delta_k^t \, \omega_{k,j}, & if\ \ j\ belongs\ to\ the\ hidden\ layer \end{cases} \qquad (31)$$

- Step 9 : Repeat steps 5 to 8 for the training vector till when the overall error become lower to the required minimal error. After sufficient repeatitions of these steps, the error can reach an acceptable value and the network is said to have been trained . It can now be used for validation and test operations [10].

Confusion matrix

The confusion matrix presents possible outcomes when measuring the intrinsic validity of a test

Table : confusion matrix

	Ill Autist patients	Neurotypic patients
Positive Test	TP	FP
Negative Test	FN	TN

- TP (true positives) represents the number of individuals effectively suffering from autism with a positive test
- FP (false positives) represents the number of non-autism patients with a positive test
- FN (false negatives) represents the number of individuals declared suffering from autism with a negative test
- TN (true negatives) represents the number of non-autisme patient with a negative test

Sensitivity : it is a measure of the actual observations that are correctly labeled (predicted), i.e, how many positive class observations are correctly labeled.

$$S_e = \frac{TP}{TP+FN}$$

Specificity : it is a measure of the actual negative observations that are correctly labeled (predicted) i.e : how many negative class observations are correctly labeled

$$S_p = \frac{TN}{TN + FP}$$

Accuracy : it is a measure of the general effectiveness of the classifier

$$Acc = \frac{TP + TN}{TP + TN + FN + FP}$$

IV. RESULTS AND DISCUSSION

4.1 Results obtained after the preprocessing of EEG signals

4.1.1 Filtering

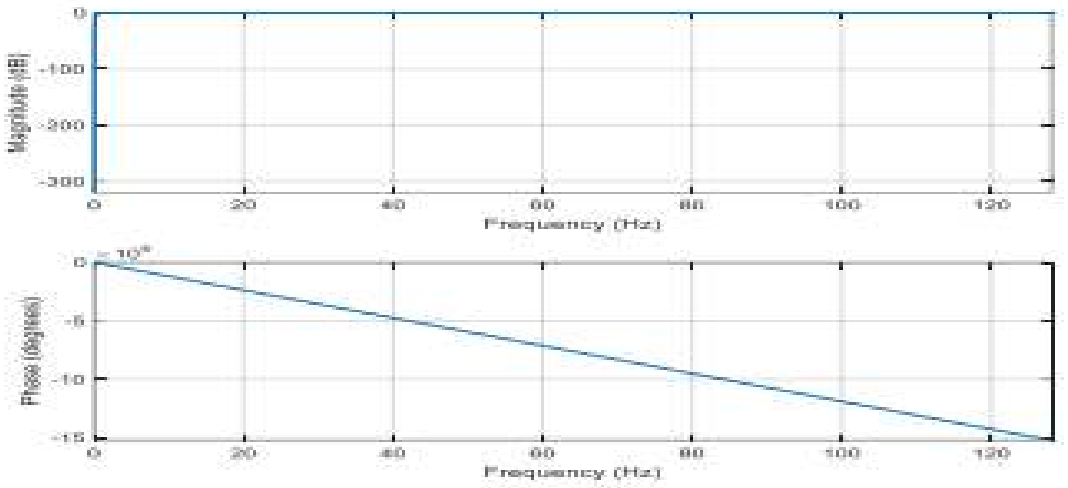

Figure 4 : Low pass filter

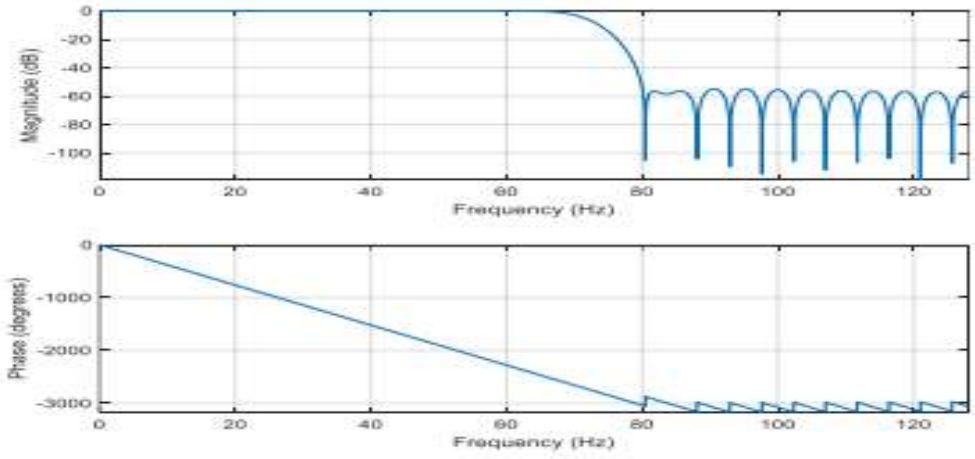

Figure 5 : high pass filter

4.2 After normalization and artifact removal

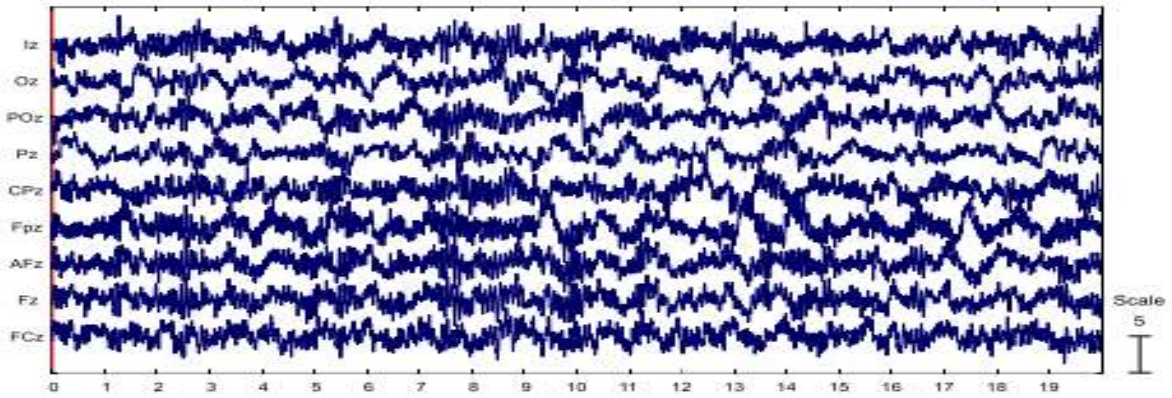

Figure 6 : EEG from Autism patient A

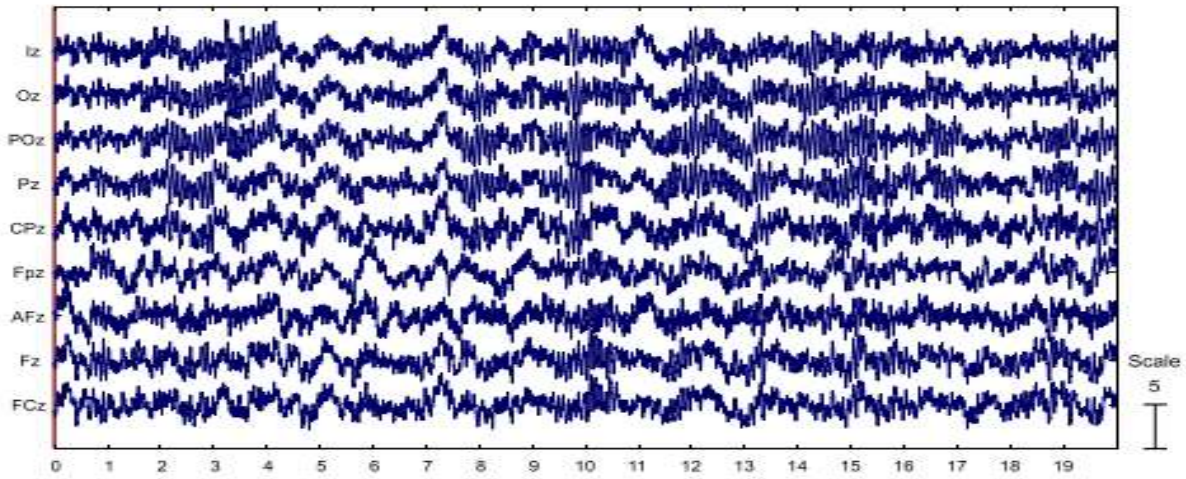

Figure 7 : EEG from a neurottypic patient B

4.3 Results obtained after frequency bands decomposition. 4.3.1 Autistic Patient

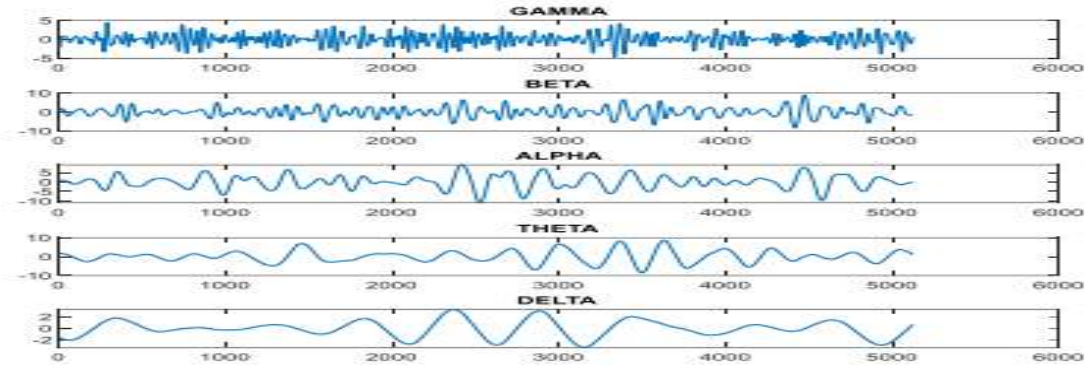

Figure 8 : Sub-bands_Decomposition from tautistic patient's EEG signal A

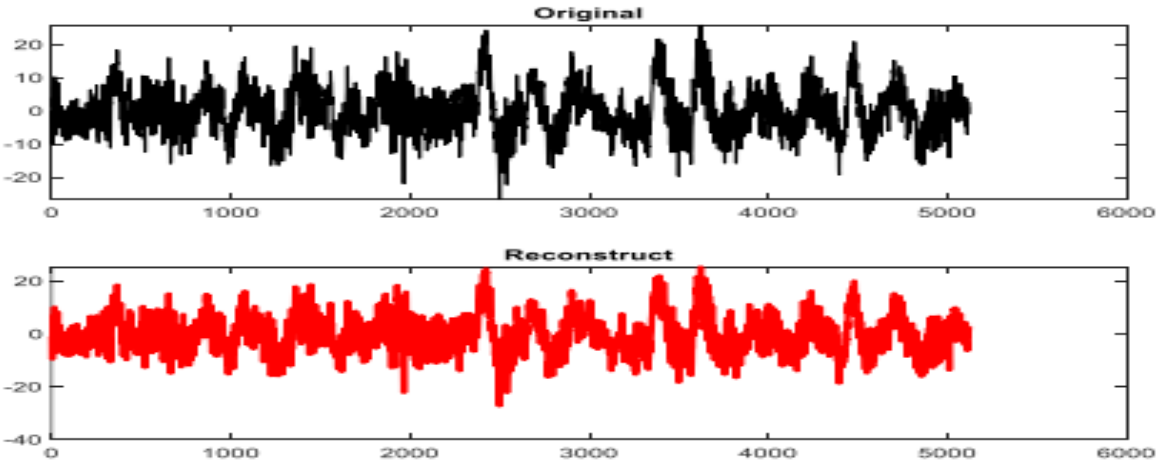

Figure 9 : Reconstruction of the decomposed signal de A

4.3.2 Neurotypic Patient

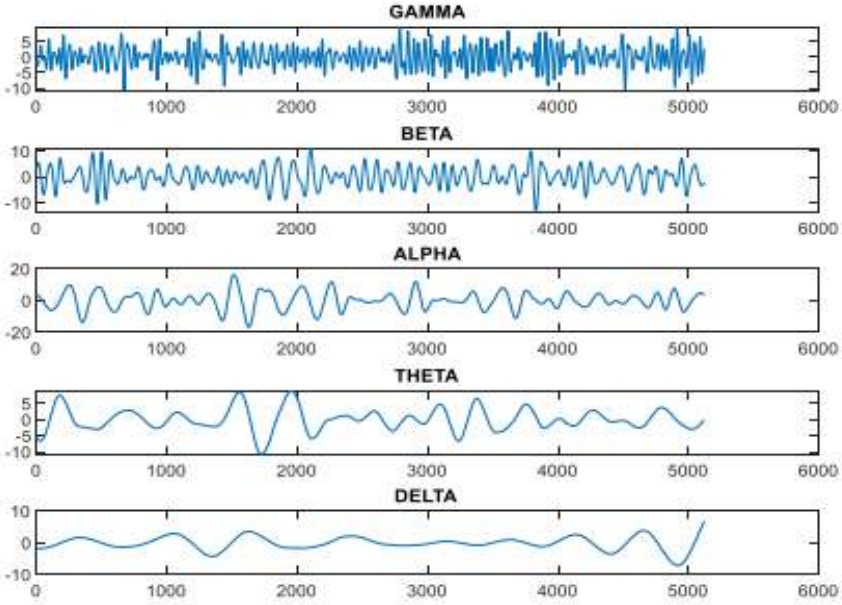

Figure 10: Sub-bands Decomposition of the neurotypic patient's EEG B

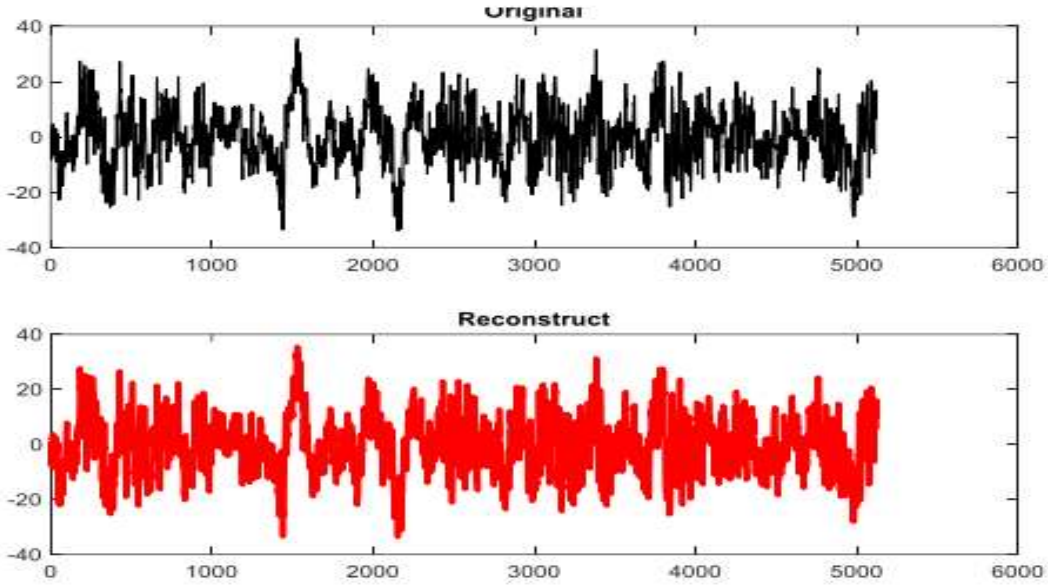

Figure 11: Reconstruction of the decomposed signal B.

4.4 Classification Results

This sub section presents results obtained for each entropic function throught confusion matrix and ROC curves..

let, Class 1 = Neurotypic patient et Class 2 = Autistic patient

4.4.1 Entropy energy logarithmic

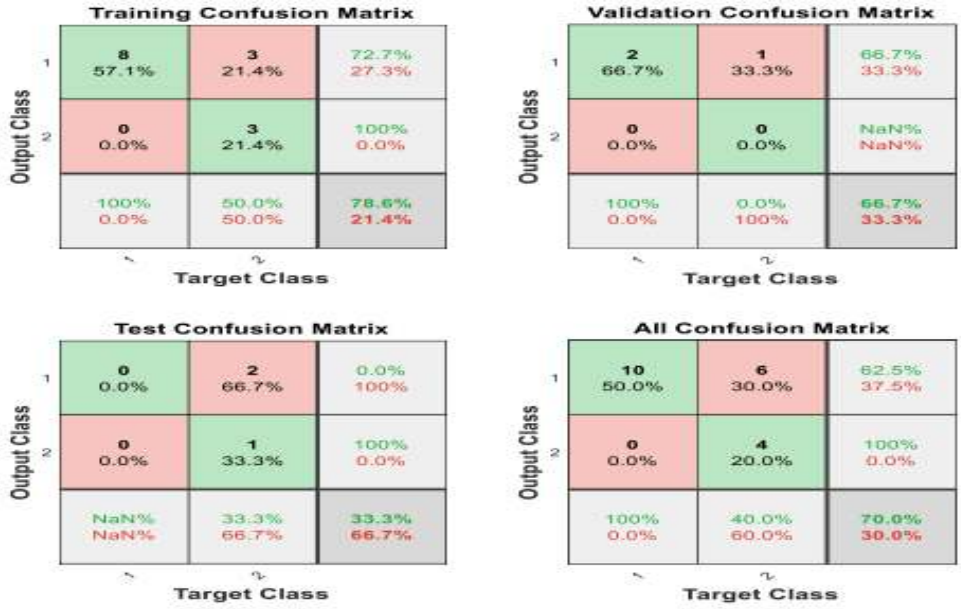

Figure 12:Confusion matrix of the logarithmic energy

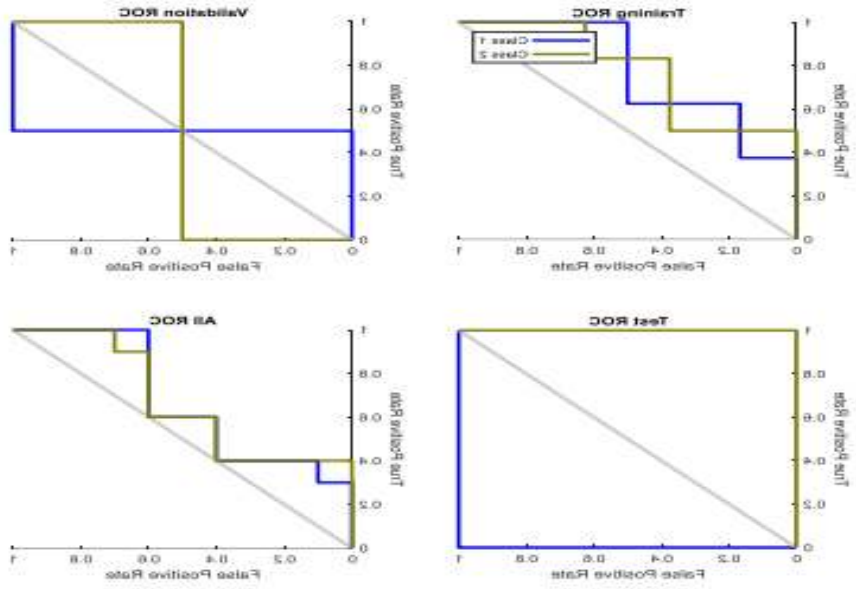

Figure 13: ROC curve of the energy logarithmic

These results shows that the Accuracy rate is at 70 % and that the erea under the ROC is grather to à 0,5 which demonstrate that the performances of the classifier are good.

Sensitivity	62,5%
Specificity	100%
Precision	70%
Positive values prediction	100%
Negative values prediction	40%

Tableau 2: Résultats, entropie d'énergie logarithmique

4.4.2 Entropy of Tsallis

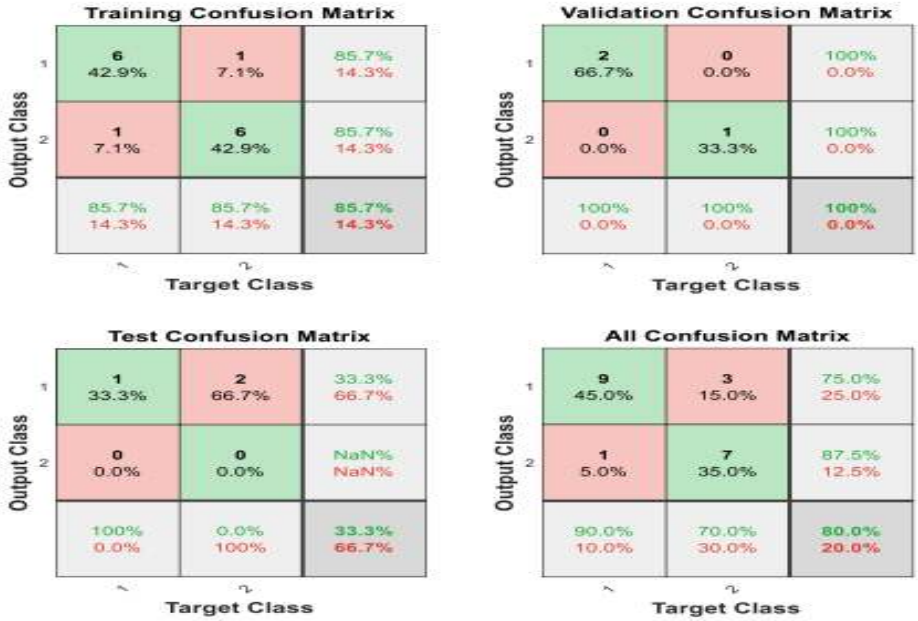

Figure 14: Matrice de confusion de Tsallis

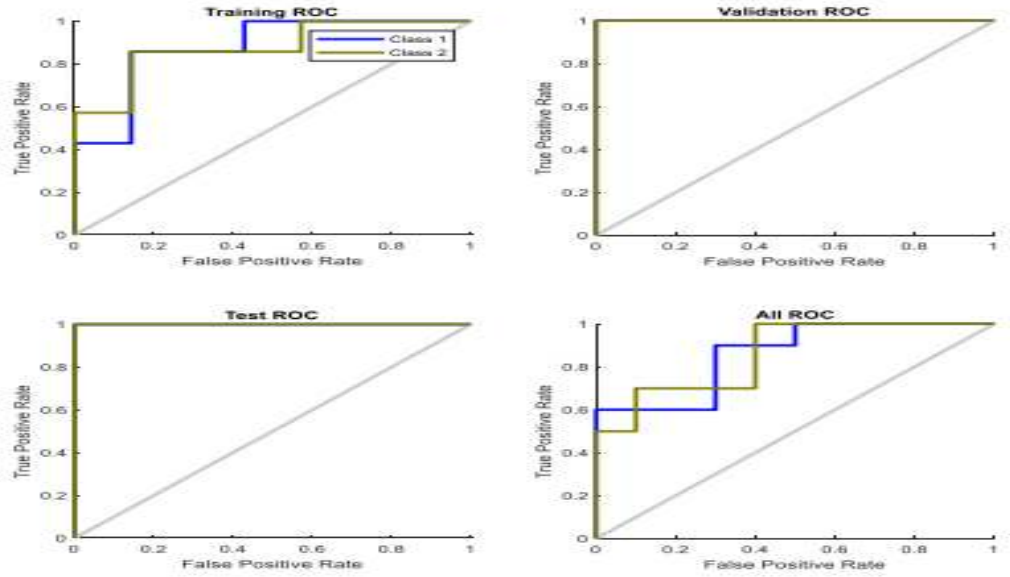

Figure 15: Courbe ROC de Tsallis

The confusion matrix of the entropy of Tsallis summarized the results on the table below

Sensitiivity	75%
Specificity	87,5%
Precision	80%
Positive values prediction	90%
Negative values prediction	70%

Tableau 3: Classification results of the entropy of Tsallis

These results shows that the classification accuracy 80 % is good .

4.4.3 Entropy of Renyi

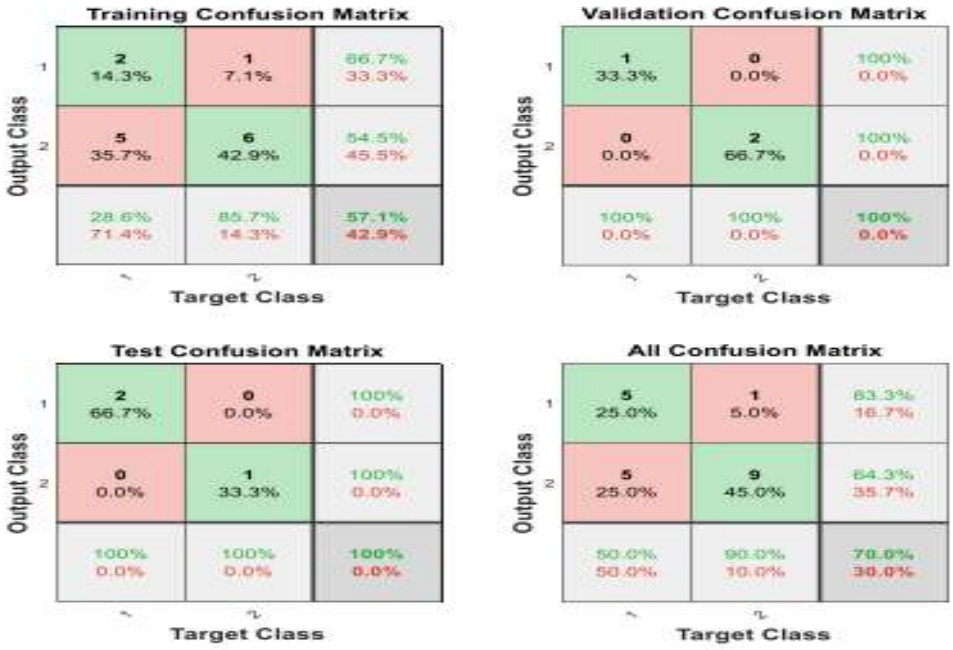

Figure 16: Confusion matrix of the entropy of Renyi

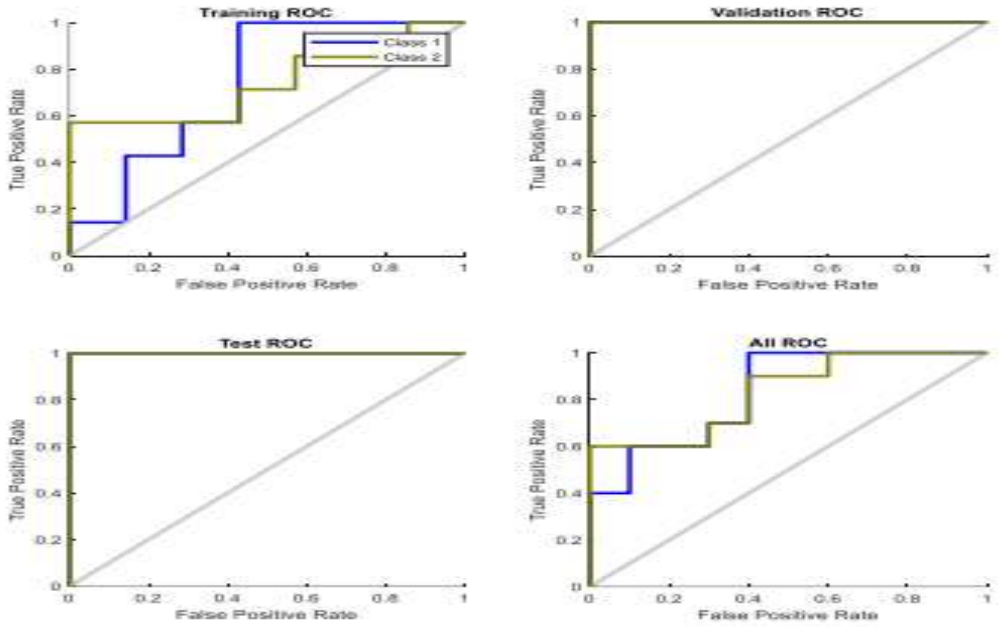

Figure 17: ROC curve of entropy of Renyi

The classification results are summarized on the table below

Sensitivity	83,3%
Specificity	64,3%
Precision	70%
Positive values prediction	50%
Negatives values prediction	90%

Tableau 4: Résultats, entropie de Tsallis

The results shows that classification accuracy is of 70 % and that the erea under the ROC curve is greather to 0,5 which means that the performances are good.

4.4.4 Entropy of Shannon

Figure 18: Confusion mtrix of Shannon

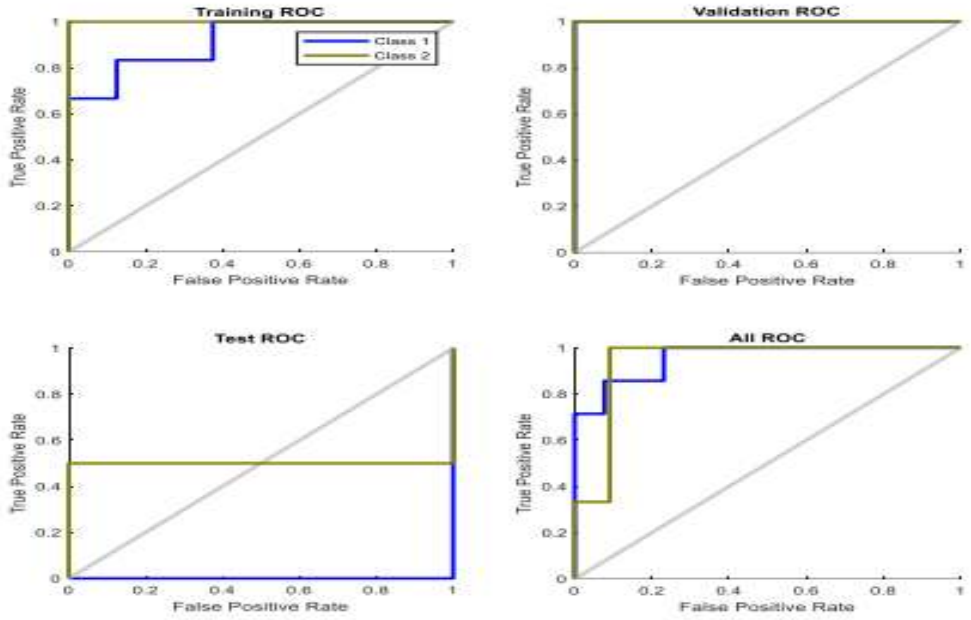

Figure 19: Courbe ROC de Shannon

Summarize results is on the table below

Sensitivity	100%
Specificity	90%
Precision	95%
Positive values prediction	90,9%
Negative values Prediction	100%

Tableau 5: Resultss, entropy of Shannon

Entropy functions	Specificity (%)	Sensitivity (%)	Precision (%)
Logarithmic Entropy	100	62,5	70
Tsallis	87,5	75	80
Renyi	64,3	83,3	70
Shannon	90	100	95

Tableau 6 : Comparative study of the precision of entropy funstions

The results show that the classification accuracy of 95 % is excellent and that the erea under the ROC curve is greather to 0,5 which mean that the performances are good.

This table shows that the four entropy functions had good precision, these performances are valid also on the ROC curve where the erea under the curve is nearly equal to 1. It is also noted that the shannon entropy give the best precision of 95 %

V. DISCUSSION

5.1 Evaluation of the best entropy the classification

The following table establish a comparative study between different entropy functions

5.2 Comparison with litterature results

Authors	Year	Feature Extraction Technique	Classifier	Dataset	Accuracy (%)
Ahmadlou et al.	2010	Wavelet + Fractal Dimension (KFD, HFD)	RBFNN	Iranian dataset	90.00
Ahmadlou et al.	2010	Wavelet + Fuzzy Synchronization Likelihood (FSL)	EPNN	Iranian dataset	—
Bosl et al.	2011	Modified Multiscale Entropy (MMSE)	SVM	USA dataset	70–100
Ahmadlou et al.	2012	Wavelet + Visibility Graph (VG)	EPNN	Iranian dataset	95.50
Alhaddad et al.	2012	Fast Fourier Transform (FFT)	FLDA	KAU dataset (KSA)	90.00
Djemal et al.	2017	DWT + Shannon Entropy	ANN	KAU dataset (KSA)	99.70
Nur Alisa Ali et al.	2020	Chi-Squared + Deep features	MLP / CNN	KAU dataset (KSA)	80.00
Baygin et al.	2021	1D-LBP + STFT + Transfer Learning	SVM	Clinical dataset	96.44
Tawhid et al.	2021	Time-frequency Spectrogram + PCA	CNN	KAU dataset (KSA)	99.15
Ari et al.	2022	Douglas-Peucker + Sparse Coding	CNN	KAU dataset (KSA)	98.88
Chawla et al.	2023	FAWT + Multiscale Permutation Entropy	CNN	Clinical dataset	98.00
Tang et al.	2024	Hybrid Graph Convolutional Network (Rest-HGCN)	GCN	ABC-CT dataset	87.12
Shi et al.	2025	STFT + Dynamic Residual Block + ACDA (TFSNet)	CNN	Sheffield / KAU	98.68
Jeyabose et al.	2026	EEG Spectrograms + XAI	Deep CNN	KAU / ACE (NIH)	—
Our work	**2026**	**DWT + Shannon Entropy**	**MLP (ANN)**	**FigShare (Sheffield)**	**98.84**

Tableau 7 : Comparaison of this work with littérature results

Table 8 presents a comprehensive comparison of the proposed method against fourteen representative state-of-the-art studies spanning over fifteen years of EEG-based ASD diagnostic research, from the pioneering contributions of Ahmadlou et al. in 2010 through the most recent deep learning-oriented frameworks published in 2025 and 2026. Several key observations emerge from this analysis.

First, the field has undergone a clear and consistent methodological evolution, transitioning from classical signal processing techniques — such as fractal dimension analysis, fast Fourier transform, and modified multiscale entropy paired with shallow classifiers — toward increasingly sophisticated deep learning architectures leveraging convolutional neural networks (CNN), graph convolutional networks (GCN), and adaptive attention-based time-frequency fusion modules. While this progression has yielded consistently high classification accuracies, often exceeding 98%, it has simultaneously introduced significant increases in model complexity, computational cost, and dataset size requirements, which may limit practical deployability in resource-constrained clinical environments.

Second, the proposed method — combining four-level Discrete Wavelet Transform (DWT) decomposition with Shannon entropy feature extraction and a Multilayer Perceptron (MLP) classifier — achieves a highly competitive accuracy of 98.84%, alongside a sensitivity of 100% and a specificity of 90%, on the FigShare (Sheffield) dataset comprising 56 subjects. This performance is particularly noteworthy given the limited cohort size compared to several competing studies, underscoring the efficiency and robustness of the proposed entropy-based pipeline under data-scarce conditions. Compared to the methodologically closest work, Djemal et al. (2017), who applied a similar DWT and Shannon entropy framework on the KAU dataset and reported 99.70% accuracy, our approach achieves comparable performance while being evaluated on an independent and more recent dataset, strengthening the generalizability of the entropy-based paradigm.

Third, while recent deep learning systems such as TFSNet (Shi et al., 2025) and the XAI-augmented CNN framework of Jeyabose et al. (2026) demonstrate impressive performance, they rely on large curated datasets, multi-stage preprocessing pipelines, and computationally intensive architectures requiring specialized GPU infrastructure for training and inference. In contrast, the proposed system operates effectively on standard computing hardware and employs a transparent, mathematically interpretable feature extraction methodology based on well-established entropy measures — a critical advantage for clinical validation, regulatory acceptance, and deployment in low-resource healthcare settings. Taken together, these results confirm that entropy-based EEG feature extraction combined with MLP classification constitutes a robust, computationally efficient, and clinically interpretable approach for automated ASD diagnosis, and that the proposed method makes a meaningful contribution to this research landscape in 2026.

CONCLUSION

This study presented a computer-aided diagnosis (CAD) system for the automated detection of autism spectrum disorder (ASD) from resting-state Electroencephalogram (EEG) signals, combining Discrete Wavelet Transform (DWT)-based frequency decomposition, entropy-driven feature extraction, and Multilayer Perceptron (MLP) neural network classification. The proposed pipeline was evaluated on a publicly available dataset of 56 subjects (28 ASD, 28 neurotypical controls) acquired via the BioSemi ActiveTwo EEG system, and demonstrated highly competitive diagnostic performance, achieving an overall classification accuracy of 98.84%, a sensitivity of 100%, and a specificity of 90% using Shannon entropy as the feature extraction function.

Four entropy measures were systematically investigated and compared — Logarithmic Energy Entropy, Tsallis Entropy, Rényi Entropy, and Shannon Entropy — with results consistently confirming the superiority of Shannon Entropy as a discriminative feature extractor for ASD classification from EEG signals. This finding is further corroborated by the comparative analysis presented in Section V, which demonstrates that Shannon Entropy-based approaches consistently yield top-tier classification performance across independent studies and datasets, as evidenced by the work of Djemal et al. (2017) and the results obtained in the present study.

Beyond its classification performance, the proposed system offers several practical advantages that distinguish it from contemporary deep learning-based approaches. First, the methodology is grounded in well-established mathematical principles — wavelet decomposition and information-theoretic entropy measures — which confer transparency, reproducibility, and ease of clinical interpretation, properties that are increasingly recognized as prerequisites for the regulatory acceptance and real-world deployment of AI-based diagnostic tools. Second, the system operates effectively on standard computing hardware without requiring specialized GPU infrastructure, rendering it particularly suitable for deployment in low-resource clinical environments, including those commonly encountered in sub-Saharan African healthcare systems. Third, the end-to-end pipeline — from EEG acquisition and preprocessing through feature extraction and classification — is computationally lightweight and time-efficient, supporting its integration into routine neurological assessment workflows.

Notwithstanding these contributions, several limitations of the present study warrant acknowledgment and motivate directions for future research. The dataset employed comprises 56 subjects, which, while sufficient to demonstrate the validity of the proposed approach, remains modest relative to the large-scale cohorts used in recent deep learning studies. Future work should therefore prioritize validation on larger, multi-site, and more demographically diverse EEG datasets to assess the generalizability and robustness of the proposed system across varying recording conditions, electrode configurations, and patient populations. Additionally, the exploration of complementary feature extraction strategies — such as functional connectivity measures, nonlinear dynamics descriptors, or hybrid entropy-connectivity feature vectors — in conjunction with more expressive classifiers, including ensemble methods or lightweight convolutional architectures, may further enhance diagnostic accuracy while preserving the computational efficiency and interpretability that characterize the present approach. Finally, the extension of the proposed framework to multi-class classification scenarios — distinguishing ASD from other neurodevelopmental disorders such as attention deficit hyperactivity disorder (ADHD) or epilepsy — represents a clinically meaningful and technically challenging direction that will be pursued in subsequent investigations.

In summary, the findings of this study confirm that entropy-based EEG feature extraction combined with MLP classification constitutes a robust, interpretable, and clinically viable approach for the automated diagnosis of autism spectrum disorder. The proposed system contributes meaningfully to the growing body of EEG-based CAD research and represents a promising foundation for the development of objective, accessible, and scalable neurophysiological diagnostic tools in both high- and low-resource clinical contexts.

REFERENCES

1. E. B. Johnson, Autism Spectrum Disorder: The Worldwide Charm and Challenge of Autism Spectrum Disorders, Special Ed. Bradford, UK: Emerald Group Publishing, 2014.
2. M. Shanda et al., "Language Ability Predicts Cortical Structure and Covariance in Boys with Autism Spectrum Disorder," Cerebral Cortex, vol. 27, no. 3, pp. 1849–1862, 2017.
3. J. Jennings Dunlap, "Autism Spectrum Disorder Screening and Early Action," Journal of the Nurse Practitioner, vol. 15, no. 7, pp. 496–501, 2019.
4. N. Fauzan and N. H. Amran, "Brain Waves and Connectivities of Autism Spectrum Disorder," Procedia — Social and Behavioral Sciences, vol. 171, pp. 882–890, 2015.
5. J. B. Ewen et al., "Decreased Modulation of EEG Oscillations in High-Functioning Autism During a Motor Control Task," vol. 10, pp. 1–10, May 2016.
6. R. Loomes, L. Hull, and W. P. L. Mandy, "What Is the Male-to-Female Ratio in Autism Spectrum Disorder? A Systematic Review and Meta-Analysis," Journal of the American Academy of Child and Adolescent Psychiatry, vol. 56, no. 6, pp. 466–474, Jun. 2017. doi: 10.1016/j.jaac.2017.03.013.
7. R. Coben, A. Clarke, W. Hudspeth, and R. Barry, "EEG Power and Coherence in Autistic Spectrum Disorder," Clinical Neurophysiology, vol. 119, no. 5, pp. 1002–1009, 2008.

8. W. Bosl, A. Tierney, H. Tager-Flusberg, and C. Nelson, "EEG Complexity as a Biomarker for Autism Spectrum Disorder Risk," BMC Medicine, vol. 9, no. 18, Feb. 2011. doi: 10.1186/1741-7015-9-18.
9. M. Ahmadlou, H. Adeli, and A. Adeli, "Fractality and a Wavelet-Chaos-Neural Network Methodology for EEG-Based Diagnosis of Autistic Spectrum Disorder," Journal of Clinical Neurophysiology, vol. 27, no. 5, pp. 328–333, Oct. 2010. doi: 10.1097/WNP.0b013e3181f40dc8.
10. M. Ahmadlou, H. Adeli, and A. Adeli, "Improved Visibility Graph Fractality with Application for the Diagnosis of Autism Spectrum Disorder," Physica A: Statistical Mechanics and its Applications, vol. 391, no. 20, pp. 4720–4726, 2012. doi: 10.1016/j.physa.2012.04.025.
11. M. Ahmadlou, H. Adeli, and A. Adeli, "Fuzzy Synchronization Likelihood-Wavelet Methodology for Diagnosis of Autism Spectrum Disorder," Journal of Neuroscience Methods, vol. 211, no. 2, pp. 203–209, Nov. 2012. doi: 10.1016/j.jneumeth.2012.08.020.
12. M. J. Alhaddad, M. Kamel, H. Malibary, E. Alsaggaf, K. Thabit, F. Dahlwi, and A. A. Hadi, "Diagnosis Autism by Fisher Linear Discriminant Analysis FLDA via EEG," 2012.
13. R. Djemal, K. AlSharabi, S. Ibrahim, and A. Alsuwailem, "EEG-Based Computer Aided Diagnosis of Autism Spectrum Disorder Using Wavelet, Entropy, and ANN," BioMed Research International, vol. 2017, Article ID 9816591, Apr. 2017. doi: 10.1155/2017/9816591.
14. S. Ibrahim, R. Djemal, and A. Alsuwailem, "Electroencephalography (EEG) Signal Processing for Epilepsy and Autism Spectrum Disorder Diagnosis," Biocybernetics and Biomedical Engineering, vol. 38, no. 1, pp. 16–26, 2018. doi: 10.1016/j.bbe.2017.08.006.
15. N. A. Ali, A. R. Syafeeza, A. S. Jaafar, M. K. M. F. Alif, and N. A. Ali, "Autism Spectrum Disorder Classification on Electroencephalogram Signal Using Deep Learning Algorithm," IAES International Journal of Artificial Intelligence, vol. 9, no. 1, pp. 91–99, Mar. 2020. doi: 10.11591/ijai.v9.i1.pp91-99.
16. J. Wang, X. Wang et al., "Increased EEG Coherence in Long-Distance and Short-Distance Connectivity in Children with Autism Spectrum Disorder," Biomedical Signal Processing and Control, 2020.
17. H. L. Green et al., "Evaluation of Mismatch Negativity as a Marker for Language Impairment in Autism Spectrum Disorder," 2020.
18. K. Gagnon, C. Bolduc et al., "REM Sleep EEG Activity and Clinical Correlates in Adults with Autism," Frontiers in Psychiatry, vol. 12, 2021.
19. M. Baygin, S. Dogan, T. Tuncer, P. D. Barua, O. Faust, N. Arunkumar, E. W. Abdulhay, E. E. Palmer, and U. R. Acharya, "Automated ASD Detection Using Hybrid Deep Lightweight Features Extracted from EEG Signals," Computers in Biology and Medicine, vol. 134, Article 104548, Jul. 2021. doi: 10.1016/j.compbiomed.2021.104548.
20. M. N. A. Tawhid, S. Siuly, H. Wang, F. Whittaker, K. Wang, and Y. Zhang, "A Spectrogram Image Based Intelligent Technique for Automatic Detection of Autism Spectrum Disorder from EEG," PLOS ONE, vol. 16, no. 6, e0253094, Jun. 2021. doi: 10.1371/journal.pone.0253094.
21. P. Garcés et al., "Resting State EEG Power Spectrum and Functional Connectivity in Autism: A Cross-Sectional Analysis," Frontiers in Neuroscience, 2022.
22. B. Ari, N. Sobahi, Ö. F. Alçin, A. Sengur, and U. R. Acharya, "Accurate Detection of Autism Using Douglas-Peucker Algorithm, Sparse Coding Based Feature Mapping and Convolutional Neural Network Techniques with EEG Signals," Computers in Biology and Medicine, vol. 143, Article 105311, Feb. 2022. doi: 10.1016/j.compbiomed.2022.105311.
23. L. B. Ribeiro and M. F. da Silva, "Systematic Review on EEG Analysis to Diagnose and Treat Autism by Evaluating Functional Connectivity and Spectral Power," Neuropsychiatric Disease and Treatment, vol. 19, pp. 415–424, 2023.
24. V. D. Thérien et al., "Different Levels of Visuospatial Abilities Linked to Differential Brain Correlates Underlying Visual Mental Segmentation Processes in Autism," Cerebral Cortex, vol. 33, no. 14, pp. 9186–9211, 2023.
25. P. Chawla, S. B. Rana, H. Kaur, and K. Singh, "Computer-Aided Diagnosis of Autism Spectrum Disorder from EEG Signals Using Deep Learning

with FAWT and Multiscale Permutation Entropy Features," Proceedings of the Institution of Mechanical Engineers, Part H: Journal of Engineering in Medicine, vol. 237, no. 2, pp. 282–294, Feb. 2023. doi: 10.1177/09544119221141751.

26. T. Tang, C. Li, S. Zhang, Z. Chen, L. Yang, Y. Mu, J. Chen, P. Xu, D. Gao, F. Li, B. He, and Y. Zhu, "A Hybrid Graph Network Model for ASD Diagnosis Based on Resting-State EEG Signals," Brain Research Bulletin, vol. 206, Article 110826, Jan. 2024. doi: 10.1016/j.brainresbull.2023.110826.
27. D. T. Atangana, G. Kenne, L. C. Djoufack, and R. Djouwe, "EEG Signal Classification Using LDA and MLP Neural Network for Automated Diagnosis," Health Informatics — An International Journal (HIIJ), vol. 9, no. 1, pp. 22–27, 2020.
28. L. Shi, L. Ma, J. Zhao, Z. Kuang, S. Wang, H. Yang, H. Wang, Q. Han, and L. Sun, "TFSNet: A Time–Frequency Synergy Network Based on EEG Signals for Autism Spectrum Disorder Classification," Brain Sciences, vol. 15, no. 7, Article 684, Jun. 2025. doi: 10.3390/brainsci15070684.
29. A. Jeyabose, A. Chadda, and V. Bhandage, "Robust and Interpretable Deep Learning on EEG Spectrograms for Autism Spectrum Disorder Detection," Journal of Computational and Cognitive Engineering, 2026. doi: 10.47852/bonviewJCCE62027780.

HOW TO CITE: Romain Atangana[1, 2, 3], Amstrong Emini Me Zenanga[3,] Aurelle Tchagna Kouanou[5], Vivien Loick Beyala Kamgang[3,6], Daniel Tchiotsop[1], Daniel Gams Massi[4], Godpromesse Kenne[1], EEG-Based Automated Diagnosis Of Autism Spectrum Disorder Using Discrete Wavelet Transform, Entropy Features And Multilayer Perceptron Neural Network, Int. J. Sci. R. Tech., 2026, 3 (6), 1331-1355. https://doi.org/10.5281/zenodo.20828901